Accurate Double Many-Body Expansion Potential Energy Surface for the Lowest Singlet State of Methylene[†]

S. Joseph and A. J. C. Varandas*

Departamento de Química, Universidade de Coimbra, 3004-535 Coimbra, Portugal

Received: December 2, 2008; Revised Manuscript Received: January 16, 2009

A single-sheeted double many-body expansion potential energy surface is reported for ground-state CH_2 by fitting accurate ab initio energies that have been semiempirically corrected by the double many-body-expansion scaled-external-correlation method. The energies of about 2500 geometries have been calculated using the multireference configuration interaction method, with the single diffusely corrected aug-cc-pV*QZ* basis set of Dunning and the full valence complete active space wave function as reference. The topographical features of the novel global potential energy surface are examined and compared with other potential energy surfaces.

1. Introduction

Methylene biradical, CH_2, is of interest to both chemists and astrophysicists. The electronic characteristics cause methylene to possess rather unusual chemical and physical properties. The ground state of methylene is a triplet state ($\tilde{X}^3B_1$) but methylene has also a low-lying singlet excited state ($\tilde{a}^1A_1$ in C_{2v} symmetry or $1^1A'$ in C_s). This appears as an electrophile and/or a nucleophile, whereas the triplet electronic state possesses radical properties. On the chemical side, methylene is a product of photolysis of diazomethane (CH_2N_2) or ketene (CH_2CO). In the interstellar medium, CH_2 plays an important role in carbon chemistry. Although the molecule has been identified[1] in interstellar space, it is the direct chemical precursor of the widely observed CH radical as well as other carbon-bearing molecules. In addition, CH_2 is thought to be an important link in the photodissociation sequence of cometary methane. Specifically, CH_4 photodissociates into CH_2, which in turn can photodissociate into CH + H or C + H_2. Of all species in this sequence, only CH has been observed. Studies on CH and CH_4 have been done in detail, with the largest uncertainty lying on the CH_2 photodissociation rate constant and branching ratio to CH + H or C + H_2.

Despite the great interest of the methylene radical in astrophysics and the chemistry of hydrocarbons combustion, there has been limited studies on the potential energy surface (PES) of the lowest (first) singlet state of methylene. However, the ground triplet state of methylene has been widely studied. Theoretically, the most accurate calculations to date on the triplet methylene PES have been conducted by Kalemos et al.[2] and Comeau et al.[3] The former[2] examines four states ($\tilde{X}^3B_1$, $\tilde{a}^1A_1$, $\tilde{b}^1B_1$, $\tilde{c}^1A_1$) of the CH_2 molecule using state-of-the-art ab initio methods and basis sets and provides clues to understand both the geometric and electronic structure of those states. The other by Comeau et al.[3] has focused on the minimum to extract the ro-vibrational energy levels of the ground and first excited states of methylene radical. Concerning the global PESs involved in the reaction $C(^3P) + H_2(^1\Sigma_g^+) \rightarrow CH(^2\Pi) + H(^2S)$, heretofore labeled as R1, a three-dimensional (3D) PES has been built for the triplet state of CH_2 by Knowles et al.[4] but their study did not attempt to describe the conical intersections between $^3B_1$ and $^3A_2$ PESs for geometries with C_{2v} symmetry, both of $^3A''$ symmetry in C_s. They have reported a C_{2v} barrier for $C(^3P)$ + H_2 insertion of ~70 kcal mol^{-1} and a C_s barrier of ~40 kcal mol^{-1}. The former result contrasts with the finding of Harding et al.[5] who found a small barrier for the insertion reaction due to the conical intersection between the two triplet surfaces. This is responsible for changing the lowest energy mechanism for reaction R1 from direct abstraction to insertion.

Concerning the reaction $C(^1D) + H_2(^1\Sigma_g^+) \rightarrow CH(^2\Pi) + H(^2S)$ (R2), a 3D PES has been calculated by Whitlock et al.[6] based on the valence-bond diatomics-in-molecules (VB-DIM) method. The reaction was predicted to follow a C_{2v} insertion mechanism with no apparent barrier against a 9.7kcal mol^{-1} barrier for the collinear abstraction. Blint and Newton[7] estimated a collinear barrier of 15kcal mol^{-1} for abstraction. Later, Bussery-Honvault et al.[8] computed an adiabatic global PES (heretofore called BHL) for the first singlet state of CH_2. Their surface shows no barrier for the C_{2v} insertion, while a barrier of 12.35 kcal mol^{-1} is present for the collinear reaction. This value lies between the VB-DIM estimation of Whitlock et al.[6] and the result of Blint and Newton.[7]

From the experimental side, a wide number of studies[9–11] have led to the determination of an accurate equilibrium geometry and a local analytical PES for the ground singlet state. However, the wealth of papers concerning the singlet−triplet energy gap shows that this splitting is subject to debate so that theses states have been intensively studied both experimentally and theoretically.

Dynamics calculations, using both the quasi-classical trajectory (QCT) and quantum mechanical methods have recently been carried out.[12–20] A more recent combined experimental and theoretical study on the dynamics of the reaction $C(^1D) + H_2$ has also been reported[21,22] using the BHL[8] for the ground singlet state PES. Unfortunately, visible discrepancies were found between the theoretical calculations on the BHL[8] surface and the experimental results. A possible explanation for these discrepancies is that the $1^1A'$[8] PES is not accurate enough in the long-range regions.[21,22] Other explanations are possible though, in particular due to the fact that there are five singlet states that correlate with $C(^1D) + H_2$ in addition to intersections of the conical type involving different electronic states.[23] In other words, nonadiabatic effects may play a significant role.

The purpose of this work is to investigate the major topographical features of the ground singlet state potential

[†] Part of the "George C. Schatz Festschrift".

* Corresponding author, varandas@qtvs1.qui.uc.pt.

10.1021/jp810600r CCC: $40.75
Published on Web 03/18/2009

energy surface of methylene by using DMBE[24–28] theory. Specifically we will employ the single-sheeted DMBE formalism which takes proper account of long-range forces. The paper is organized as follows. Section 2 describes the ab initio calculations carried out in the present work. In section 3, we deal with the analytical representation of the PES. While section 3.1 focuses on the two-body energy terms, section 3.2 concentrates on the three-body ones. The main topographical features of the DMBE potential energy surface are discussed in section 4. The concluding remarks appear in section 5.

2. Ab Initio Calculations

The ab initio calculations have been carried out at the MRCI[29] level using the full valence complete active space[30] (FVCAS) wave function as reference. Such a FVCAS reference wave function, which involves six correlated electrons in six active orbitals ($5a' + 1a''$), amounts to a total of 50 configuration state functions. For the basis set, we have selected the aug-cc-pVQZ (heretofore denoted by AVQZ) of Dunning,[31,32] with the calculations being carried out using the Molpro[33] package. About 2500 grid points were chosen to map the potential energy surface of both the C−H_2 and H−CH regions. The former region is defined by $1.0 \le r_{H_2}/a_0 \le 4.0$, $1.2 \le R_{C-H_2}/a_0 \le 10.0$ and $0.0 \le \gamma/\text{deg} \le 90$ while, for the H−CH one, we have used a grid defined by $1.5 \le r_{CH}/a_0 \le 4.0$, $1.0 \le R_{H-CH}/a_0 \le 10.0$, and $0.0 \le \gamma/\text{deg} \le 180$. For both channels, r, R, and γ define the associated atom−diatom Jacobi coordinates.

All calculated ab initio energies have been subsequently corrected by the double many-body-expansion scaled-external-correlation[34] (DMBE-SEC) method to account for excitations beyond singles and doubles and, most importantly, for the incompleteness of the basis set. The total DMBE-SEC interaction energy is then written as

$$V(\mathbf{R}) = V_{\text{FVCAS}}(\mathbf{R}) + V_{\text{SEC}}(\mathbf{R}) \quad (1)$$

where

$$V_{\text{FVCAS}}(\mathbf{R}) = \sum_{\text{AB}} V^{(2)}_{\text{AB,FVCAS}}(R_{\text{AB}}) + V^{(3)}_{\text{ABC,FVCAS}}(R_{\text{AB}}, R_{\text{BC}}, R_{\text{AC}}) \quad (2)$$

$$V_{\text{SEC}}(\mathbf{R}) = \sum_{\text{AB}} V^{(2)}_{\text{AB,SEC}}(R_{AB}) + V^{(3)}_{\text{ABC,SEC}}(R_{\text{AB}}, R_{\text{BC}}, R_{\text{AC}}) \quad (3)$$

and $R = \{R_i\}$ ($i = 1-3$) defines the set of interatomic coordinates. In turn, the first two terms of the SEC series expansion assume the form

$$V^{(2)}_{\text{AB,SEC}}(R_{\text{AB}}) = \frac{V^{(2)}_{\text{AB,FVCAS-CISD}}(R_{\text{AB}}) - V^{(2)}_{\text{AB,FVCAS}}(R_{\text{AB}})}{F^{(2)}_{\text{AB}}} \quad (4)$$

$$V^{(3)}_{\text{ABC,SEC}}(R_{\text{AB}}, R_{\text{BC}}, R_{\text{AC}}) = \frac{V^{(3)}_{\text{ABC,FVCAS-CISD}}(R_{\text{AB}}, R_{\text{BC}}, R_{AC}) - V^{(3)}_{\text{ABC,FVCAS}}(R_{\text{AB}}, R_{\text{BC}}, R_{\text{AC}})}{F^{(3)}_{\text{ABC}}} \quad (5)$$

Following previous work,[34] the $F^{(2)}_{\text{AB}}$ parameter in eq 4 has been chosen to reproduce the bond dissociation energy of the corresponding AB diatomic, while $F^{(3)}_{\text{ABC}}$ has been estimated as the average of the two-body F factors. Such a procedure leads to the following values: $F^{(2)}_{\text{HH}} = 0.9773$ and $F^{(2)}_{\text{CH}} = 0.9098$, and $F^{(3)}_{\text{CHH}} = 0.9323$. Note that the calculated scaling factors are close to unit, which is accepted as a good requirement for the method to yield accurate results.

3. Single-Sheeted Potential Energy Surface

Following early developments by Murrell and Carter,[35] we have recently suggested[36] a switching function formalism to approximate a multivalued potential energy surface by a single-sheeted form. For the title system, the spin-spatial Wigner−Witmer rules predict the following dissociation scheme

$$\begin{aligned} \text{CH}_2(1^1A') &\rightarrow \text{H}_2(^1\Sigma_g^+) + \text{C}(^1D) \\ &\rightarrow \text{H}_2(^3\Sigma_u^+) + \text{C}(^3P) \\ &\rightarrow \text{CH}(^2\Pi) + \text{H}(^2S) \end{aligned} \quad (6)$$

Clearly, a proper description of the potential energy surface would imply the use of a multisheeted formalism due to the occurrence of two electronic states for the carbon atom. Since we are mostly interested in the dissociation channel of $CH_2(1^1A')$ into $H_2(^1\Sigma_g^+)$ + C(^1D), and CH($^2\Pi$) dissociates into C(^3P) + H(^2S), one must use a function that switches off the C(^3P) state in the C + H_2 dissociation channel. For this purpose, we have suggested[36] the form

$$h(R_1) = \sum_{i=1}^{2} \{1 - \tanh[\alpha_i(R_1 - R_1^{i0}) + \beta_i(R_1 - R_1^{i1})^3]\} \quad (7)$$

where R_1 represents the H−H distance, and α_i and β_i ($i = 1, 2$) are parameters to be calibrated from the ab initio energies such as to control the C(^1D−^3P) decay with increasing H−H distance (see the left panel of Figure 1). A major advantage of this switching formalism over the one originally proposed by Murrell and Carter[35] is that it leads to a unique set of electronic states at the three-atom asymptote.

In order to get a smooth three-body energy term, we multiply $h(R_1)$ by an amplitude function that annihilates eq 7 at short-range regions (small C−H_2 distances)

$$g(r_1) = \frac{1}{2}\{1 + \tanh[\alpha(r_1 - r_1^0)]\} \quad (8)$$

where r_1 is the distance of C to the center of mass of H_2. The parameters in $g(r_1)$ have been chosen so as to diminish any abrupt switching behavior in the short-range part (see right-hand-side panel of Figure 1). The complete switching function has the form

$$f(\mathbf{R}) = g(r_1)h(R_1) \quad (9)$$

with the numerical values of the parameters in eqs 7−9 being collected in Table 1.

Within DMBE theory, the total potential energy function is expressed as

$$V(\mathbf{R}) = V^{(1)}_{\text{C}(^1D)} f(\mathbf{R}) + \sum_{i=1}^{3} [V^{(2)}_{\text{EHF}}(R_i) + V^{(2)}_{\text{dc}}(R_i)] + [V^{(3)}_{\text{EHF}}(\mathbf{R}) + V^{(3)}_{\text{dc}}(\mathbf{R})] \quad (10)$$

where $V^{(1)}_{\text{C}(^1D)}$ is the energy (at the scaled AVQZ level) difference between C(^1D) and C(^3P) electronic states, namely, $V^{(1)}_{\text{C}(^1D)} = 0.046604E_{\text{h}}$. The following sections give the details of all other analytical energy terms in eq 10.

3.1. Two-Body Energy Terms. The potential energy curves of CH and H_2 have been obtained using the extended Hartree−Fock approximate correlation energy method for diatomic molecules, including the united atom limit[37] (EHFACE2U)

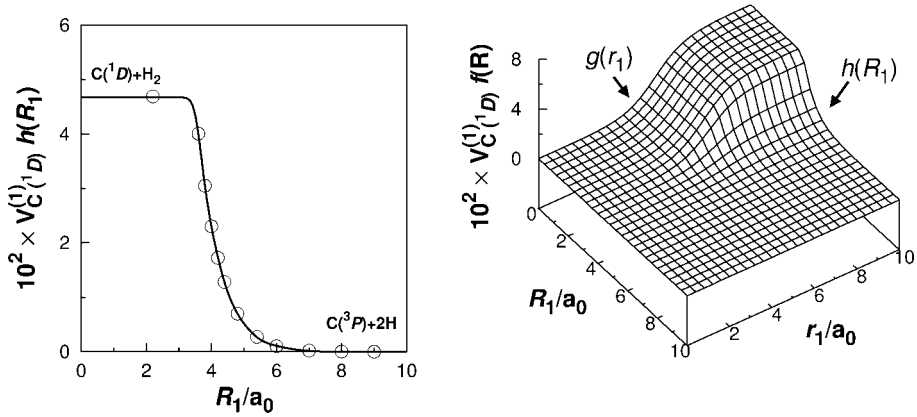

Figure 1. Switching function used to model the single-sheeted CH_2 DMBE potential energy surface. Shown in the left panel is the fit of the $h(R_1)$ switching form to the ab initio points points calculated for C + H_2 as a function of H−H distance (R_1). Shown in the right-hand side panel is a perspective view of the global switching function in eq 9.

TABLE 1: Parameters in the Switching Function of Equations 7−9

α_1	0.571350
α_2	0.705610
β_1	1.001760
β_2	0.138958
R_1^{10}	2.315740
R_1^{11}	4.689200
R_1^{20}	3.846300
R_1^{21}	5.714090
α	0.75
r_1^0	5.5

which shows the correct behavior at the asymptotic limits. They assume the general form[37]

$$V(\mathbf{R}) = V_{\mathrm{EHF}}(\mathbf{R}) + V_{\mathrm{dc}}(\mathbf{R}) \tag{11}$$

where EHF refers to the extended Hartree−Fock type energy and dc is the dynamical correlation energy. This is modeled semiempiricaly as described[38]

$$V_{\mathrm{dc}}(R) = -\sum_{n=6,8,10} C_n \chi_n(R) R^{-n} \tag{12}$$

where

$$\chi_n(R) = \left[1 - \exp\left(-A_n \frac{R}{\rho} - B_n \frac{R^2}{\rho^2}\right)\right]^n \tag{13}$$

In eq 13, A_n and B_n are auxiliary functions[24,25] defined by $A_n = \alpha_0 n^{-\alpha_1}$ and $B_n = \beta_0 \exp(-\beta_1 n)$ where α_0, α_1, β_0, and β_1 are universal dimensionless parameters for all isotropic interactions: $\alpha_0 = 16.36606$, $\alpha_1 = 0.70172$, $\beta_0 = 17.19338$, and $\beta_1 = 0.09574$. In turn, $\rho = 5.5 + 1.25R_0$ is a scaling parameter, $R_0 = 2(\langle r_A^2\rangle^{1/2} + \langle r_B^2\rangle^{1/2})$ is the LeRoy[39] parameter for onset the undamped R^{-n} expansion, and $\langle r_X^2\rangle$ is the expectation value of the square radius for the outermost electrons of atom X (X = A, B).

The exponentially decaying part of the EHF type energy is represented by the general form

$$V_{\mathrm{EHF}}(R) = -\frac{D}{R}(1 + \sum_{i=1}^{n} a_i r^i) \exp(-\gamma r) \tag{14}$$

where

$$\gamma = \gamma_0[1 + \gamma_1 \tanh(\gamma_2 r)] \tag{15}$$

and $r = R - R_e$ is the displacement from the equilibrium diatomic geometry. In turn, D, a_i, and γ_i ($i = 1,..., n$) are adjustable parameters to be obtained as described elsewhere.[25,37] Here, we employed the accurate EHFACE2U potential energy function for $H_2(X^1\Sigma_g^+)$ reported elsewhere.[40] To get the potential energy curve of $CH(^2\Pi)$ in Figure,2 we used the same method,[37] and those ab initio points calculated at the same level of theory used for the title system. The numerical values of all parameters for both diatomic potentials are collected in Table 1 of the Supporting Information.

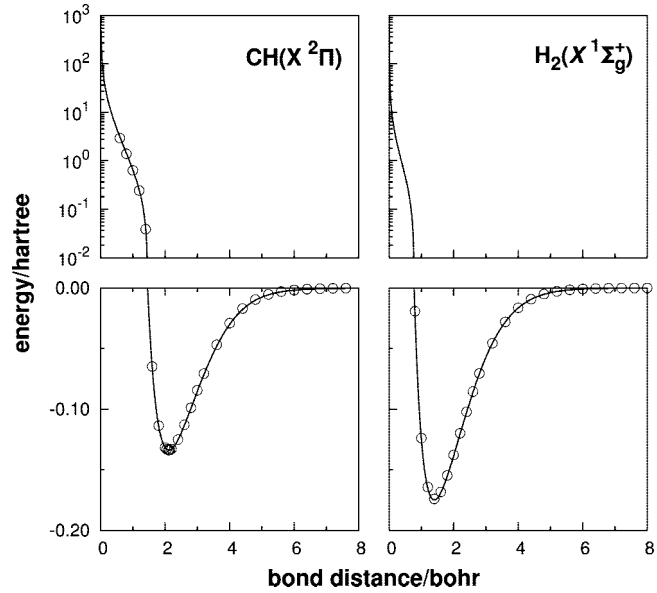

Figure 2. EHFACE2U potential energy curves for $CH(^2\Pi)$ and $H_2(^1\Sigma_g^+)$. The solid circles correspond to the ab initio points calculated at the present level of theory.

3.2. Three-Body Energy Terms. ***3.2.1. Three-Body Dynamical Correlation Energy.*** The three-body dynamical correlation energy assumes the usual form[40]

$$V_{\mathrm{dc}}^{(3)} = \sum_i \sum_n f_i(R) C_n^{(i)}(R_i, \theta_i) \chi_n(r_i) r_i^{-n} \tag{16}$$

where i labels the I-JK channel associated with the center of mass separation and (r_i, θ_i, R_i) are the Jacobi coordinates corresponding to a specific $\mathbf{R} = (R_1, R_2, R_3)$ geometry of the triatomic system (see Figure 1 of ref 26. Moreover, f_i is a switching function chosen from the requirement that its value must be +1 at $R_i = R_i^e$ and $r_i \to \infty$ and 0 when $R_i \to \infty$. The three-body switching function assumes the form $f_i = (1/2)\{1 - \tanh[\xi(\eta R_i - R_j - R_k)]\}$, with corresponding

TABLE 2: Stratified Root-Mean-Square Deviations (kcal mol^{-1}) of DMBE Potential Energy Surface

energy	N^a	max dev^b	rmsd	$N_{>\text{rmsd}}{}^c$
10	150	0.264	0.120	50
20	197	0.716	0.196	47
30	232	1.738	0.299	43
40	263	1.906	0.365	57
60	347	2.056	0.501	81
80	469	2.056	0.559	127
100	884	3.591	0.677	200
140	1875	5.989	0.797	386
200	2422	5.989	0.838	488
250	2451	5.989	0.843	491
1000	2510	5.989	0.858	512

[a] Number of calculated DMBE-SEC points up to the indicated energy range. [b] Maximum deviation up to indicated energy range. [c] Number of calculated DMBE-SEC points with an energy deviation larger than the root-mean-square deviation (rmsd).

expressions applying for f_j and f_k. Following a recent proposal[41] to correct the long-range behavior, we adopt $\eta = 6$ and ξ to be equal to $1.0a_0^{-1}$. Regarding the damping function $\chi_n(r_i)$, we still adopt eq 13 but replace R by the center-of-mass separation for the relevant atom−diatom channel. In addition, the value of ρ has been optimized by trial-and-error to get a good asymptotic behavior of the dynamical correlation term, leading to $\rho = 16.125a_0$.

The atom−diatom dispersion coefficients in eq 16, which are given by

$$C_n^{(i)}(R_i) = \sum_L C_n{}^L(R) P_L(\cos\theta_i) \tag{17}$$

where $P_L(\cos\theta_i)$ denotes the Lth Legendre polynomial. The expansion in eq 17 has been truncated by considering of only the coefficients $C_6{}^0$, $C_6{}^2$, $C_8{}^0$, $C_8{}^2$, $C_8{}^4$, and $C_{10}{}^0$; all other coefficients have been supposed to make insignificant contributions and hence neglected. To estimate the dispersion coefficients we have employed the generalized Slater−Kirkwood formula,[42] with the dipolar polarizabilities calculated in the present work at the MRCI/AVQZ level of theory. As usual, the atom−diatom dispersion coefficients so calculated for a set of internuclear distances were fitted to the form

$$C_n^{L,\text{A-BC}}(R) = C_n^{L,\text{AB}} + C_n^{L,AC} + D_M\left(1 + \sum_{i=1}^{3} a_i r^i\right)\exp\left(-a_1 r - \sum_{i=2}^{3} b_i r^i\right) \tag{18}$$

where $C_n^{L,\text{AB}}$, for $L = 0$, are the corresponding diatom dispersion coefficients (see Table 2 of the Supporting Information; for $L \neq 0$ $C_n^{L,\text{AB}} = 0$). All parameters and coefficients in eq 18 have been explained elsewhere.[41] The parameters that resulted from such fits are also reported in Table 2 of the Supporting Information, whereas the internuclear dependences of the dispersion coefficients are shown in Figure 3. Note that in $R = 0$ the asymptotic limit for the isotropic component of the dispersion coefficients are fixed in the value for the A−X interaction, with X being the united atom of BC. As noted elsewhere,[40] eq 16 causes an overestimation of the dynamical correlation energy at the atom−diatom dissociation channels. To correct such a behavior, we have multiplied the two-body dynamical correlation energy for the ith pair by $\prod_{j\neq i}(1 - f_j)$ and correspondingly for the channels j and k. This ensures[40] that the only two-body contribution at the ith channel is the one of the JK diatom.

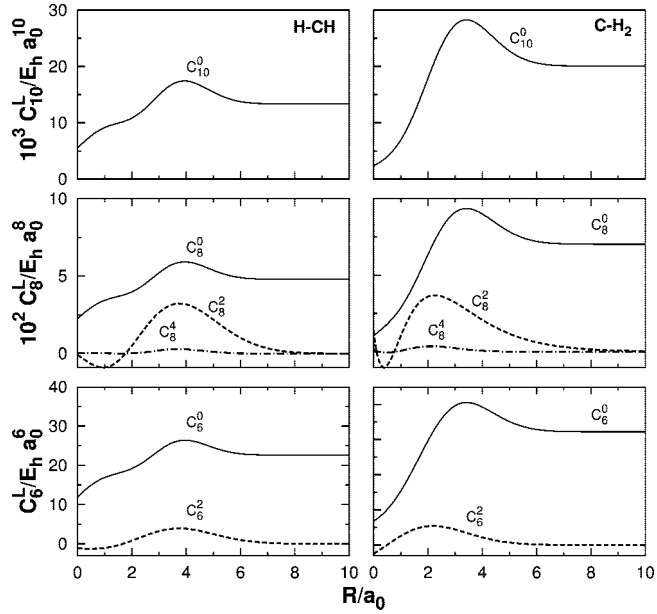

Figure 3. Dispersion coefficients for the atom−diatom asymptotic channels of CH_2 as a function of the corresponding internuclear distance of the diatom.

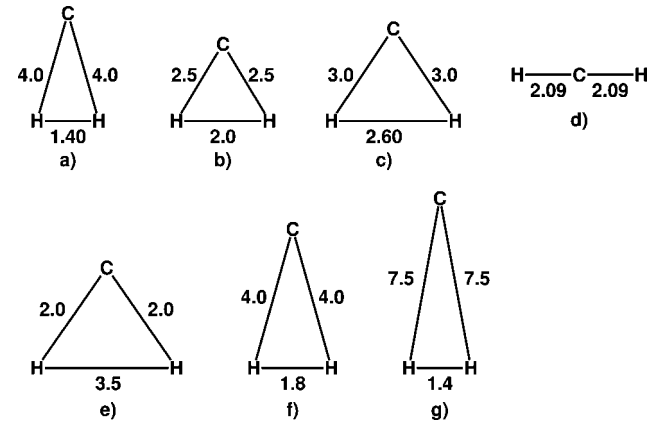

Figure 4. Reference geometries used in the present work for the three-body EHF part of the potential energy surface. See tex for details.

3.2.2. Three-Body Extended Hartree−Fock Energy. By removing, for a given triatomic geometry, the sum of the one-body and two-body energy terms from the corresponding DMBE-SEC interaction energies eq 1, which was defined with respect to the infinitely separated ground-state atoms, one obtains the total three-body energy. By further subtracting the three-body dynamical correlation contribution eq 16 from the total three-body energy that is calculated in that way, one obtains the three-body extended Hartree−Fock energy. This will be represented by the following three-body distributed-polynomial[43] form

$$V_{\text{EHF}}^{(3)} = \sum_{j=1}^{7} P^j(Q_1, Q_2, Q_3)\prod_{i=1}^{3}\{1 - \tanh[\gamma_i^j(R_i - R_i^{j,\text{ref}})]\} \tag{19}$$

where $P^j(Q_1, Q_2, Q_3)$ is a sixth-order polynomial form in symmetry coordinates which are defined as usual.[44–46] Figure 4 displays the reference geometries that define the displacement coordinates used to write the EHF-type polynomials in eq 19. As usual, we obtain the reference geometries $R_i^{j,\text{ref}}$ by first assuming their values coincide with bond distances of the

TABLE 3: Stationary Point Properties of the $CH_2(1^1A')$ PES

feature	property	ab initio[a]	ab initio[b]	BHL[c]	RKHS[d]	DMBE	others
$C(^1D) + H_2$	R_1/a_0	1.40	1.402	1.40	1.40	1.401	1.401[f]
	V/E_h		−0.1260(−0.1284[l])			−0.12787(−0.1281[m])	
	ΔE^e	0.0	0.0	0.0	0.0	0.0	0.0
	ω(H−H)/cm^{-1}	4430	4399	4420	4418	4396	4403[f]
CH + H	R_2/a_0	2.12	2.12	2.12	2.12	2.12	2.12[g]
	V/E_h		−0.1320 (−0.1338[l])			−0.13373 (−0.1339[m])	−0.1337[h]
	ΔE^e	−3.82	−3.76 (−3.38[l])	−3.86	−3.85	−3.68 (−3.61[m])	−3.80[i], −3.73[n] (−3.83[o])
	ω(C−H)/cm^{-1}	2851	2848	2848	2850	2845	2861[g]
linear barrier	R_1/a_0			1.85	1.85	1.85	
C−H−H	R_2/a_0			2.56	2.55	2.55	
	R_3/a_0						
	V/E_h					−0.1069	
	ΔE^e			12.36	12.37	13.2	
	ω_1 (H−H)/cm^{-1}			4565	4341	2624	
	ω_2 (C−H)/cm^{-1}			1454	1454	1515	
	ω_3 (bend)/cm^{-1}			1117	1117	1232	
global minimum	R_1/a_0	3.27	3.2578	3.26	3.27	3.2682	3.020[j]
	R_2/a_0	2.09	2.0957	2.09	2.09	2.0972	2.097[j]
	R_3/a_0	2.09	2.0957	2.09	2.09	2.0972	2.097[j]
	V/E_h		−0.28472			−0.28725	0.2889[k]
	ΔE^e	−99.70	−99.5 (−99.2[l])	−99.8	−99.75	−100.01 (−99.75[m])	−89.5[i], −98.9[n] (−100.3[o])
	ω_1 (C−H)/cm^{-1}	2801	2915	2923	2906	2914	2806[j]
	ω_2 (C−H)/cm^{-1}	2955	2990	3136	3069	2994	2865[j]
	ω_3 (bend)/cm^{-1}	1331	1396	1383	1382	1393	1352[j]

[a] Reference 8. [b] This work MRCI. [c] Reference 8. [d] Reference 13. [e] Relative to the $C(^1D) + H_2$ asymptote (kcal mol^{-1}). [f] Reference 58. [g] Reference 59. [h] Reference 68. [i] Reference 6. [j] Reference 47. [k] Reference 3. [l] This work, MRCI(Q). [m] This work, DMBE-SEC. [n] Reference 23 MRCI. [o] Reference 23 MRCI(Q).

associated stationary points. Subsequently, we relax this condition via a trial-and-error least-squares fitting procedure. Similarly, the nonlinear range-determining parameters γ_i^j have been optimized in this way. The complete set of parameters amounts to a total of 140 linear coefficients (c_i; see the definition in the Supporting Information), 21 nonlinear coefficients γ_i^j, and 7 reference geometries $R_i^{j,\mathrm{ref}}$. Their optimal numerical values are collected in Tables 3 and 4 of the Supporting Information. A total of 2500 points has been used for the calibration procedure, with the energies covering a range up to 500 kcal mol^{-1} above the CH_2 global minimum. Table 2 shows the stratified root-mean-squared deviation (rmsd) values of the final potential energy surface with respect to all the fitted ab initio energies. As shown, the fit shows a maximum rmsd of 0.9 kcal mol^{-1} up to the highest repulsive energy stratum.

4. Features of DMBE Potential Energy Surface

We find no barrier for the $C(^1D)$ insertion into H_2 in the $1^1A'$ PES of CH_2, although for collinear geometries the DMBE function predicts a barrier height of 13.2 kcal mol^{-1} with respect to the $C(^1D) + H_2$ asymptote, which is located at $R_1 = 1.85a_0$ and $R_2 = 2.55a_0$. This result lies between the early theoretical estimates of 9.7[6] and 15.0[7] kcal mol^{-1}, while being in fairly good agreement with the most recent theoretical predictions of 12.35 kcal mol^{-1} (from the BHL[8] PES) and 12.3 kcal mol^{-1} (from the RKHS[13] PES).

The DMBE PES here reported shows a calculated well depth of 180.25 kcal mol^{-1} for the CH_2 complex, in its lowest singlet state relative to the three atom dissociation limit, also in good agreement with the best theoretical determination of 180.3 kcal mol^{-1} by Comeau et al.[3] Comparing to the BHL[8] PES calculated with the MR-SDCI method and a LANO (local atomic natural orbital) basis set, the DMBE PES predicts a well depth larger by 2.05 kcal mol^{-1}. Note that the calculated MRCI/AVQZ well depth for the $1^1A'$ state of CH_2 is 178.66 kcal mol^{-1}, with the Davidson correction (Q) leading to a further increase of 1.12 kcal mol^{-1}. Note further that the scaling of the dynamical correlation using the DMBE-SEC method leads to a well depth of 180.25 kcal mol^{-1}. Furthermore, we have performed computationally expensive MRCI/AV5Z calculations for some selected geometries, having obtained a well depth of 179.19 kcal mol^{-1}. As seen, this is smaller by 0.59 kcal mol^{-1} than the MRCI(Q) value and 1.06 kcal mol^{-1} than our estimate based on DMBE-SEC. Since this accounts for the finiteness of both the one electron basis set and CI expansion, it seems appropriate that this method predicts a further lowering of 0.47 kcal mol^{-1} with respect to the Davidson (Q) correction. We find the potential well in DMBE to be located at $R = 1.3a_0$ and $r = 3.26a_0$, which corresponds to a geometry of C_{2v} symmetry with R(C−H) $= 2.09a_0$ and ∠HCH $= 102.4°$. Clearly, these results are in very good agreement with the available experimental[47] data on CH_2, R(C−H) $= 2.09a_0$ and ∠HCH $= 102.4°$. Relative to the entrance channel, the calculated well depth of CH_2 (100.01 kcal mol^{-1}) in Table 3 is seen to be larger by about 10 kcal mol^{-1} than the early valence-bond prediction of Whitlock et al.[6] but in good agreement with the more recent predictions of 99.8 kcal mol^{-1} from BHL[7] and 99.75 kcal mol^{-1} from RKHS[13] PESs.

Table 3 also shows that the harmonic frequencies of the DMBE PES are in good agreement with the calculated raw MRCI/AVQZ values of 2915, 2990, and 1396 cm^{-1}, with the corresponding DMBE-SEC values being 2914, 2994, and 1393 cm^{-1}. In fact, the deviations between the DMBE predicted values and the MRCI ones are smaller (5 cm^{-1} or less) than the corresponding differences for the BHL and RKHS PESs.

The singlet state minimum is located slightly higher than the triplet ground-state one. The separation between these two states has been widely studied both theoretically[48–51] and experimentally,[3,52–54] but the values obtained cover a wide range of energies[55] (from 874.39 to 3427.61 cm^{-1}) depending on the method employed. We find the calculated MRCI/AVQZ value for T_0,

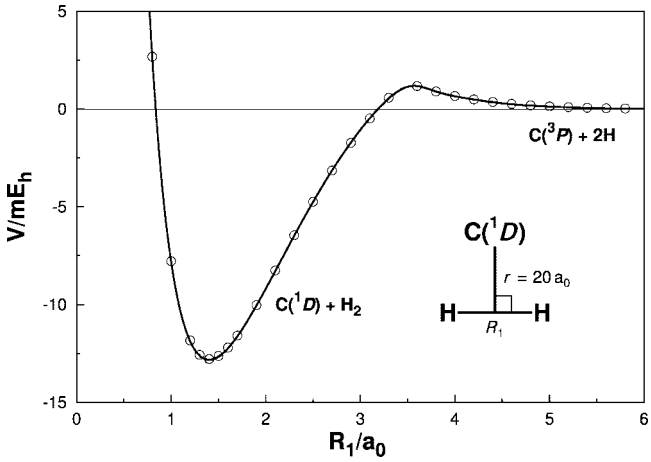

Figure 5. Potential energy curve of the one body term [$C(^1D)-C(^3P)$] referring to the excitation energy.

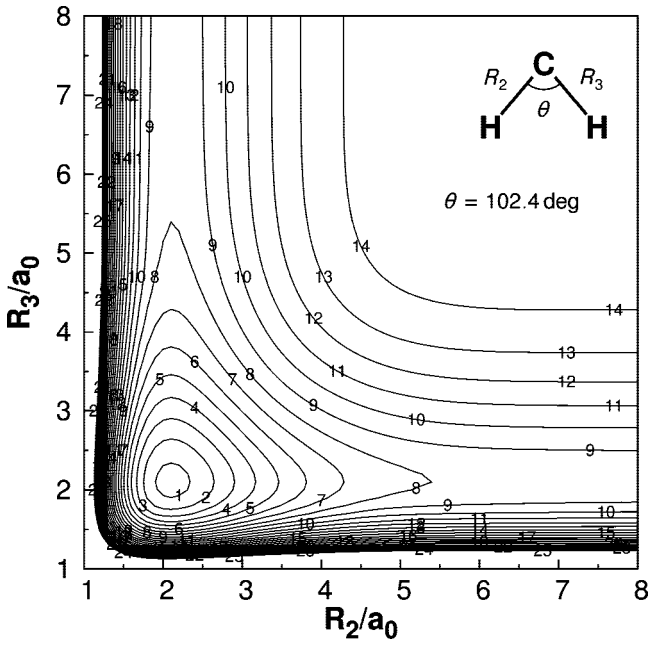

Figure 6. Contour plot for bond stretching H−C−H keeping the included angle fixed at 102.4°. Contours are equally spaced by $0.02E_h$ starting at $-0.28E_h$.

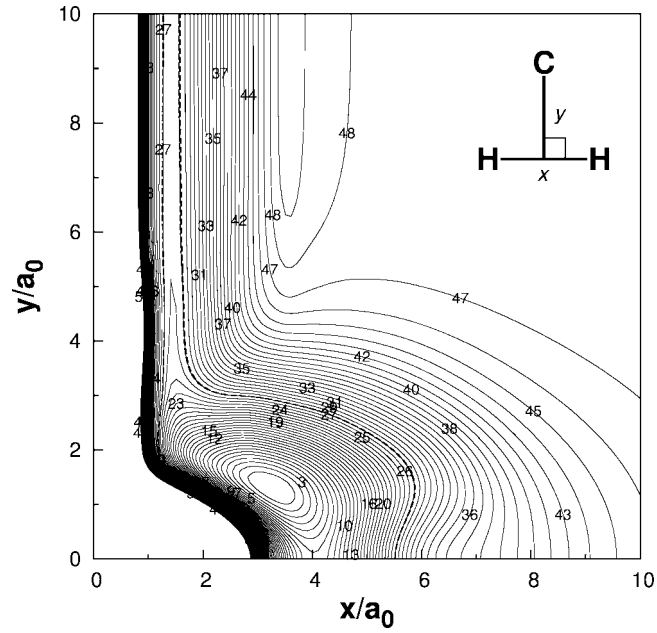

Figure 7. Contour plot for a C_{2v} insertion of C atom into diatomic H_2. Contours are equally spaced by $0.006E_h$, starting at $-0.28E_h$. The dashed lies are contours equally spaced by $0.000075E_h$, starting at $-0.127E_h$.

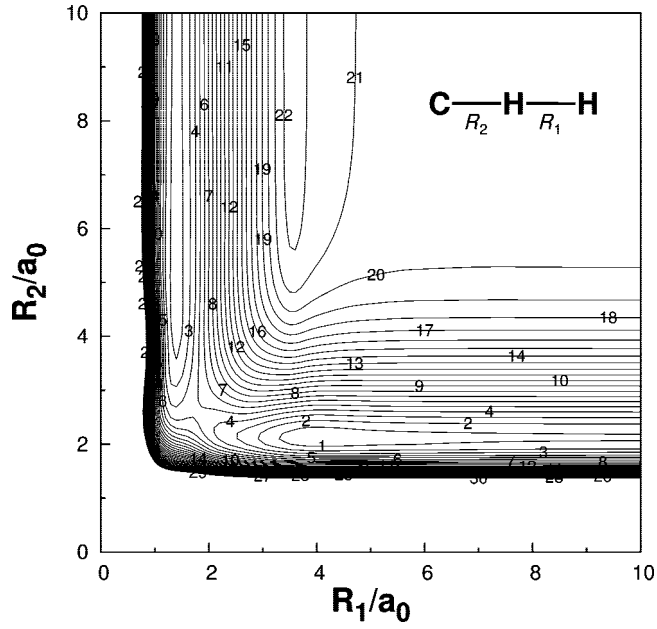

Figure 8. Contour plot for bond stretching C−H−H in linear configuration. Contours are equally spaced by $0.00675E_h$, starting at $-0.268E_h$.

3115.94 cm^{-1}, to be in good agreement with the best experimental determination of[56,57] 3147 ± 5 cm^{-1}.

Figures 5−10 illustrate the major topographical features of the CH_2 DMBE PES which has been calculated in the present work. Clearly, it has a smooth and correct behavior over the whole configuration space. Figure 6 presents the contour plot of the PES for a fixed internal angle ∠HCH = 102.4°. It shows that the exit channel presents no potential barrier toward dissociation of CH_2 into $CH(^2\Pi) + H(^2S)$. Figures 7 and 8 represents the contour plots corresponding to the insertion and abstraction of $C(^1D) + H_2$ reaction. Specifically, Figure 8 shows that the potential at collinear geometries rises rapidly up to a barrier of 13.2 kcal mol^{-1}. So, the reaction $C(^1D) + H_2(^1\Sigma_g^+) \rightarrow CH(^2\Pi) + H(^2S)$ is expected to occur mainly via noncollinear configurations. Figure 9 shows energy contours for a carbon [$C(^1D)$] atom moving around a ground-state hydrogen molecule, while a corresponding plot for a hydrogen atom moving around CH is presented in Figure 10. The salient features from these plots are some of the most relevant stationary points for the title system. A characterization of their attributes (geometry, energy, and vibrational frequencies) is reported in Table 3. Also included for comparison are the results that have been obtained from other PESs, ab initio calculations, and experimental spectroscopic measurements.[6,47,58,59]

The range of barrier heights for linearity in the $1^1A'$ state of CH_2 obtained by ab initio calculation is pretty large,[60] varying from 8000 to 10000 cm^{-1}. For example, an early calculation[61] using the rigid bender Hamiltonian gave a result of 10000 cm^{-1} while another one employing[62] the internally contracted MRCI method using a FVCAS with an extended Gaussian basis set and including also the Renner−Teller coupling effect gave a result of 8800 cm^{-1}. Furthermore, a high level ab initio calculation employing[3] also the MRCI method with a ANO basis

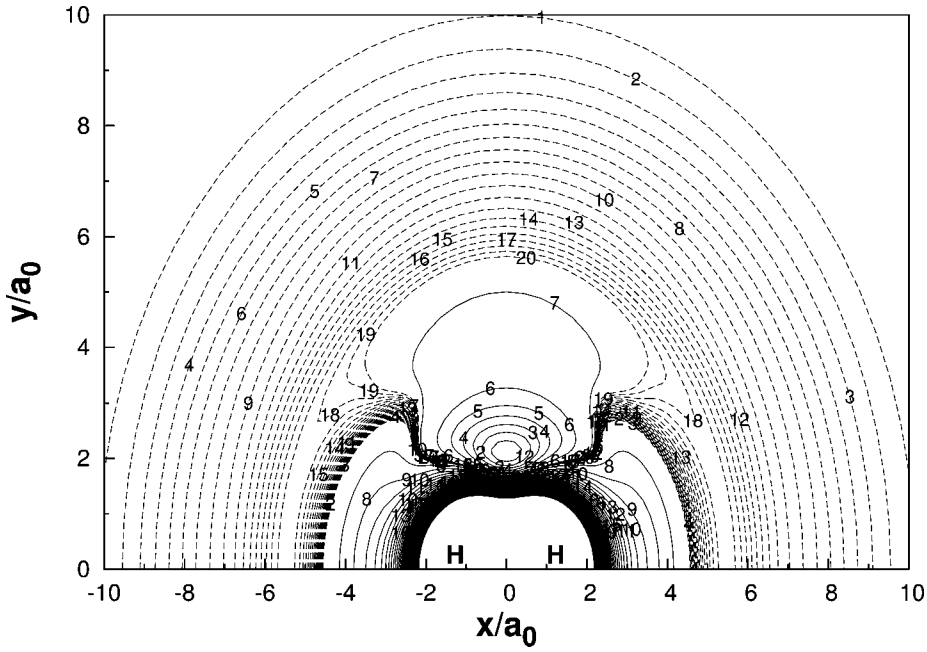

Figure 9. Contour plot for an C atom moving around a fixed H_2 diatomic in equilibrium geometry $R_1 = 1.401a_0$ which lies along the *X*-axis with the center of the bond fixed at the origin. Contours are equally spaced by $0.005E_h$, starting at $-0.17E_h$. The dashed lies are contours equally spaced by $0.000075E_h$, starting at $-0.128E_h$.

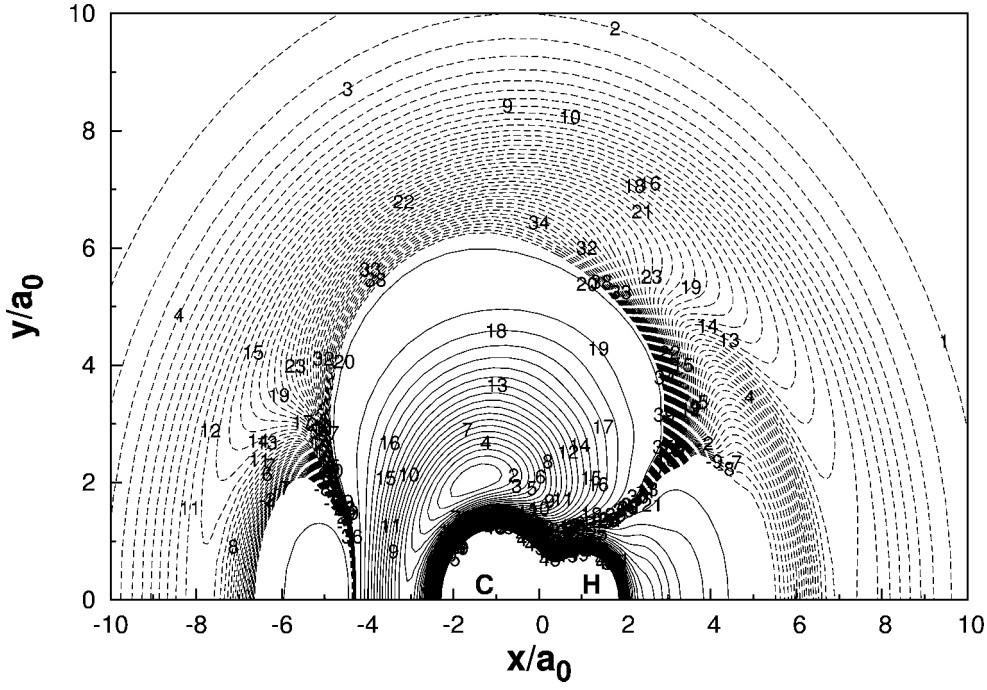

Figure 10. Contour plot for an H atom moving around a fixed CH diatomic $R_{CH} = 2.12a_0$, which lies along the *X*-axis with the center of the bond fixed at the origin. Contours are equally spaced by $0.0075E_h$, starting at $-0.287E_h$. The dashed lines are contours equally spaced by $0.000075E_h$, starting at $0.133E_h$.

set but without inclusion of the Renner−Teller coupling gave a barrier height of 9600 cm^{-1}. In turn, the DMBE PES predicts for the barrier to linearity in $1^1A'$ CH_2 (see Figure 11) a height of 9644 cm^{-1}, a value in good agreement with the experimental determination of 9800 cm^{-1} by Duxbury and Jungen[63] obtained by fitting a bending potential function to the $(0, v_2, 0)$ levels for $v_2 = 0-3$ as observed in laser-induced fluorescence (LIF)[64,65] and low-resolution dispersed fluorescence[66] experiments.

The isotropic and leading anisotropic potentials are two important quantities for the study of scattering processes in the $1^1A'$ CH_2 PES and are shown in Figure 12. The isotropic average potential V_0 determines how close on average the atom and molecule can approach each other, while the magnitude of V_2 indicates whether or not the molecule prefers to orient its axis along the direction of the incoming atom: a negative value prefers the collinear approach while a positive one favors the approach through an isosceles triangular geometry.

Finally, preliminary rate constant calculations have been carried out for the reaction $C(^1D) + H_2 \rightarrow CH + H$ by running quasi-classical trajectories on the PES of the present work at a temperature of 298 K. The calculations predict the rate constant to be $(1.34 \pm 0.06) \times 10^{-10}$ cm^3 s^{-1} when the vibrational and

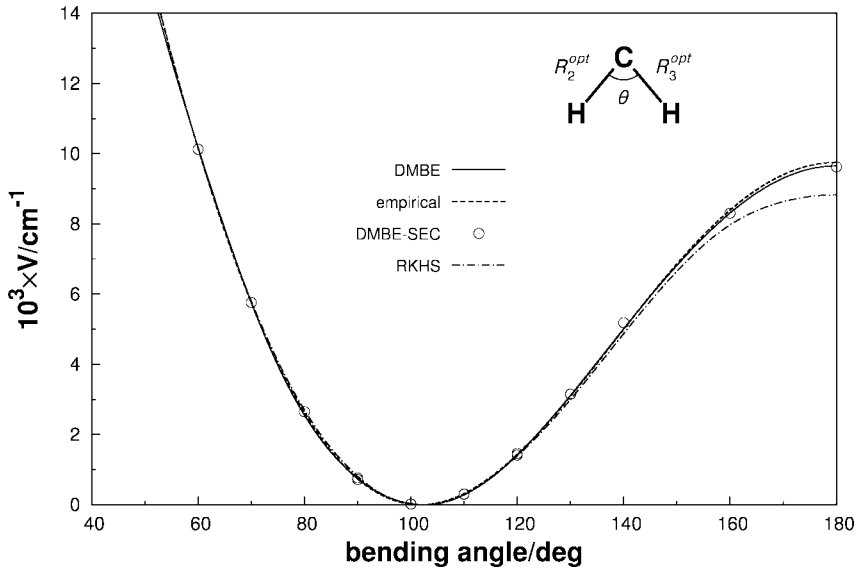

Figure 11. Optimized C_{2v} bending curve of CH_2 as a function of bending angle. The continuous line refers to DMBE (this work), dashed line to RKHS,[13] and dotted line to empirical data.[63]

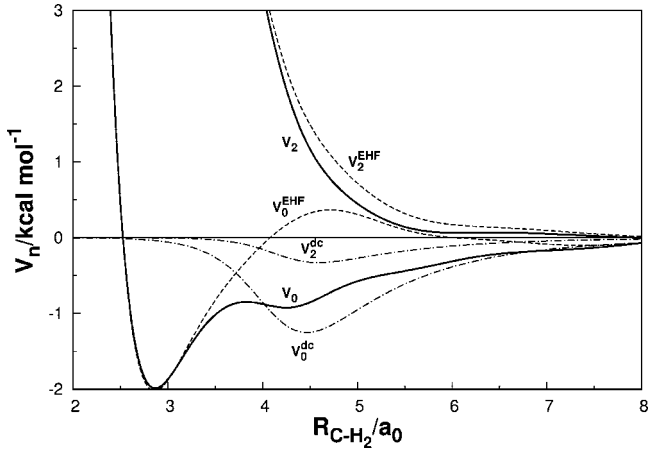

Figure 12. Isotropic (V_0) and leading anisotropic (V_2) components of the C−H_2 interaction potentials, with the diatomic molecule fixed at the equilibrium geometry. Continuous lines represent V_0 and V_2 components of DMBE PES; dash-dot and dashed lines are the corresponding three-body dynamical correlation and EHF parts.

rotational quantum numbers of H_2 are kept fixed at $v = 0$ and $j = 0$. This shows good agreement with a recent state-specific quantum dynamics result[16] on the RKHS[13] surface, $(1.2 \pm 0.6) \times 10^{-10}$ cm^3 s^{-1}, and the experimental[67] value of $(2.0 \pm 0.6) \times 10^{-10}$ cm^3 s^{-1}. The calculated thermalized rate constant is $(1.09 \pm 0.06) \times 10^{-10}$ cm^3 s^{-1}. Although only slightly off the experimental error bar, we should recall that quantum effects are ignored in the present estimate. A detailed account of the ongoing dynamics calculations will be reported elsewhere.

5. Concluding Remarks

In this work, we have calculated a wealth of accurate MRCI energies for the first singlet state of the methylene biradical, which have subsequently been corrected using the DMBE-SEC method and modeled analytically using DMBE theory. The global DMBE PES so obtained shows good behavior over the entire configuration space. Its various topographical features have also been carefully examined and compared with the corresponding attributes of other PESs, as well as experimental data available in the literature. The good agreement observed with the rate constant values reported in the literature recommends it for future dynamics studies of the title reaction.

Acknowledgment. This work has the support of Fundacao para a Ciencia e Tecnologia, Portugal: POCI/QUI/60501/2004 and REEQ/128/QUI/2005, under the auspices of POCI 2010 of Quadro Comunitário de Apoio III cofinanced by FEDER.

Supporting Information Available: Tables of numerical values of all parameters for both diatomic potentials, parameters in eq 18, and the three-body extended Hartree−Fock energy in eq 19 and reference geometries of the extended Hartree−Fock energy in Eq 19, and definition of the general three-body EHF polynomial. This material is available free of charge via the Internet at http://pubs.acs.org.

References and Notes

(1) Hollis, J. M.; Jewell, P. R.; Lovas, F. J. *Astrophys. J.* **1995**, *438*, 259.
(2) Kalemos, A.; Dunning, T. H., Jr.; Mavridis, A.; Harrison, J. F. *Can. J. Chem.* **2004**, *82*, 684.
(3) Comeau, D. C.; Shavitt, I.; Jensen, P.; Bunker, P. R. *J. Chem. Phys.* **1989**, *90*, 6491.
(4) Knowles, P. J.; Handy, N. C.; Carter, S. *Mol. Phys.* **1983**, *49*, 681.
(5) Harding, L. B.; Gudagnini, R.; Schatz, G. C. *J. Phys. Chem.* **1993**, *97*, 5472.
(6) Whitlock, P. A.; Muckerman, J. T.; Kroger, P. M. *Potential Energy Surfaces and Dynamics Calculations*; Truhlar, D. G., Ed.; Plenum: New York, 1981; p 551.
(7) Blint, R. J.; Newton, M. D. *Chem. Phys. Lett.* **1975**, *32*, 178.
(8) Bussery-Honvault, B.; Honvault, P.; Launay, J.-M. *J. Chem. Phys.* **2001**, *115*, 10701.
(9) Jensen, P.; Bunker, P. R. *J. Chem. Phys.* **1988**, *89*, 1327.
(10) Sears, T. J. *J. Chem. Phys.* **1986**, *85*, 3711.
(11) Marshall, M. D.; McKellar, A. R. W. *J. Chem. Phys.* **1986**, *85*, 3716.
(12) Banares, L.; Aoiz, F.; Honvault, P.; Bussery-Honvault, B.; Launay, J.-M. *J. Chem. Phys.* **2003**, *118*, 565.
(13) Banares, L.; Aoiz, F.; Vázquez, S. A.; Ho, T. S.; Rabitz, H. *Chem. Phys. Lett.* **2003**, *374*, 243.
(14) Rackham, E. J.; Gonzalez-Lezana, T.; Manolopoulos, D. E. *J. Chem. Phys.* **2003**, *119*, 12895.
(15) Lin, S. Y.; Guo, H. *J. Chem. Phys.* **2003**, *119*, 11602.
(16) Lin, S. Y.; Guo, H. *J. Phys. Chem. A* **2004**, *108*, 2141.
(17) Lin, S. Y.; Guo, H. *J. Phys. Chem. A* **2004**, *108*, 10066.
(18) Mouret, L.; Launay, J.-M.; Terao-Dunseath, M.; Dunseath, K. *Phys. Chem. Chem. Phys.* **2004**, *6*, 4105.
(19) Bussery-Honvault, B.; Julien, J.; Honvault, P.; Launay, J.-M. *Phys. Chem. Chem. Phys.* **2005**, *7*, 1476.

(20) Lin, S. Y.; Guo, H.; Farantos, S. C. *J. Chem. Phys.* **2005**, *122*, 124308.
(21) Balucani, N.; Capozza, G.; Cartechini, L.; Bergeat, A.; Bobbenkamp, R.; Casaveechia, P.; Aoiz, J. F.; Banares, L.; Honvault, P.; Bussery-Honvault, B.; Launay, J. *Phys. Chem. Chem. Phys.* **2004**, *6*, 4957.
(22) Balucani, N.; Capozza, G.; Segoloni, E.; Bobbenkamp, R.; Casaveechia, P.; Gonzalez-Lezana, T.; Rackham, E. J.; Banares, L.; Aoiz, J. F. *J. Chem. Phys.* **2005**, *122*, 234309.
(23) Liu, X. J.; Bian, W. S.; Zhao, X.; Tao, X. T. *J. Chem. Phys.* **2006**, *125*, 074306.
(24) Varandas, A. J. C. *J. Mol. Struct.: THEOCHEM* **1985**, *120*, 401.
(25) Varandas, A. J. C. *Adv. Chem. Phys.* **1988**, *74*, 255.
(26) Varandas, A. J. C. *Chem. Phys. Lett.* **1992**, *194*, 333.
(27) Varandas, A. J. C. *Reaction and Molecular Dynamics: Proceedings of the European School on Computational Chemistry*; Laganá, A., Riganelli, A., Eds.; Lecture Notes in Chemistry 75; Springer: Berlin, 2000; pp 33.
(28) Varandas, A. J. C.; Voronin, A. I. *Mol. Phys.* **1995**, *85*, 497.
(29) Werner, H.-J.; Knowles, P. J. *J. Chem. Phys.* **1988**, *89*, 5803.
(30) Werner, H.-J.; Knowles, P. J. *Chem. Phys. Lett.* **1985**, *115*, 259.
(31) Dunning, T. H., Jr. *J. Chem. Phys.* **1989**, *90*, 1007.
(32) Kendall, R. A.; Dunning, T. H., Jr.; Harrison, R. J. *J. Chem. Phys.* **1992**, *96*, 6796.
(33) MOLPRO is a package of ab initio programs written by H.-J. Werner and P. J. Knowles, with contributions from Almlöf, J. Amos, R. D. Deegan, M. J. O. Elbert, S. T. Hampel, C. Meyer, W. Peterson, K. A. Pitzer, R. Stone, A. J. Taylor, P. R. Lindh. R. 1998.
(34) Varandas, A. J. C. *J. Chem. Phys.* **1989**, *90*, 4379.
(35) Murrell, J. N.; Carter, S. *J. Phys. Chem.* **1984**, *88*, 4887.
(36) Varandas, A. J. C.; Poveda, L. *Theor. Chem. Acc.* **2006**, *116*, 404.
(37) Varandas, A. J. C.; Silva, J. D. *J. Chem. Soc., Faraday Trans.* **1992**, *88*, 941.
(38) Varandas, A. J. C. *Mol. Phys.* **1987**, *60*, 527.
(39) Le Roy, R. J. *Spec. Period. Rep.: Chem. Soc. Mol. Spectrosc.* **1973**, *1*, 113.
(40) Varandas, A. J. C. *J. Chem. Phys.* **1996**, *105*, 3524.
(41) Varandas, A. J. C.; Rodrigues, S. P. J. *J. Phys. Chem. A* **2006**, *110*, 485.
(42) Matías, M. A.; Varandas, A. J. C. *Mol. Phys.* **1990**, *70*, 623.
(43) Martínez-Nuñez, E.; Varandas, A. J. C. *J. Phys. Chem.* **2001**, *105*, 5923.
(44) Murrell J. N.; Carter S.; Farantos, S. C.; Huxley, P.; Varandas A. J. C. *Molecular Potential Energy Functions*; Wiley: New York, 1984.
(45) Murrell, J. N.; Sorbie, K.; Varandas, A. J. C. *Mol. Phys.* , *32*, 1359.
(46) Farantos, S.; Leisengang, E. C.; Murrell, J. N.; Sorbie, K.; Teixeira-Dias, J. J. C.; Varandas, A. J. C. *Mol. Phys.* , *34*, 947.
(47) Herzberg, G. *Molecular Spectra and Molecular Structure. III Electronic Spectra and Electronic Structure of Polyatomic Molecules*; Van Nostrand: New York, 1966.
(48) Shih, S. K.; Peyerimhoff, S. D.; Buenker, R. J.; Peric, M. *Chem. Phys. Lett.* **1978**, *55*, 206.
(49) Romelt, J.; Peyerimhoff, S. D.; Buenker, R. *J. Chem. Phys.* **1981**, *54*, 147.
(50) Bunker, P. R.; Jensen, P.; Kraemer, W. P.; Beardsworth, R. *J. Chem. Phys.* **1986**, *85*, 3724.
(51) C, W.; Bauschlicher, J.; Langhoff, S. R.; Taylor, P. R. *J. Chem. Phys.* **1987**, *87*, 387.
(52) Gaspar, P. P.; Hammond, G. S. *Carbenes*; Jones, M., Moss, R. A., Eds.; Wiley: New York, 1975; Vol. 2.
(53) Zittel, P. F.; Ellison, G. B.; O'Neil, S. V.; Herbst, E.; Lineberger, W. C.; Reinhardt, W. P. *J. Am. Chem. Soc.* **1976**, *98*, 3731.
(54) McKellar, A. R. W.; Bunker, P. R.; Sears, T. J.; Evenson, K. M.; Saykally, R. J.; Langhoff, S. R. *J. Chem. Phys.* **1983**, *79*, 5251.
(55) Shavitt, I. *Tetrahedron* **1985**, *41*, 1531.
(56) Jensen, P.; Bunker, P. R. *J. Chem. Phys.* **1988**, *89*, 1327.
(57) Gu, J.; Hirsch, G.; Buenker, R. J.; Brumm, M.; Osmann, G.; Bunker, P. R.; Jensen, P. *J. Mol. Struct.* **2000**, *517*, 247.
(58) Rosen, B. *International Tables of Selected Constants*; Pergamon: New York, 1970; Vol. 17.
(59) Zachwieja, M. *J. Mol. Spectrosc.* **1995**, *170*, 285.
(60) Schaefer, H. F. *Science* **1986**, *231*, 1100.
(61) Bunker, P. R.; Landsberg, B. M. *J. Mol. Spectrosc.* **1977**, *67*, 374.
(62) Green, W. H.; Handy, N. C.; Knowles, P. J.; Carter, S. *J. Chem. Phys.* **1991**, *94*, 118.
(63) Duxbury, G.; Jungen, C. *Mol. Phys.* **1988**, *63*, 981.
(64) Petek, H.; Nesbitt, D. J.; Darwin, D. C.; Moore, C. B. *J. Chem. Phys.* **1987**, *86*, 1172.
(65) Petek, H.; Nesbitt, D. J.; Moore, C. B.; Birss, F. W.; Ramsay, D. A. *J. Chem. Phys.* **1987**, *86*, 1189.
(66) Feldmann, D.; Meier, K.; Schmiedl, R.; Welge, K. H. *Chem. Phys. Lett.* **1978**, *60*, 30.
(67) Sato, K.; Ishida, N.; Kurakata, T.; Iwasaki, A.; Tsunashima, S. *Chem. Phys.* **1998**, *237*, 195.
(68) Huber, K. P.; Herzberg, G. *Molecular Spectra and Molecular Structure. IV Constants of Diatomic Molecules*; Van Nostrand: New York, 1979.

JP810600R